Journal of
Marine Science
and Engineering

MDPI

Article

Near-Trapping on a Four-Column Structure and the Reduction of Wave Drift Forces Using Optimized Method

Guanghua He [1,2], Zhigang Zhang [3], Wei Wang [1,*], Zhengke Wang [3] and Penglin Jing [1]

1 School of Naval Architecture and Ocean Engineering, Harbin Institute of Technology, Weihai 264209, Shandong, China; ghhe@hitwh.edu.cn (G.H.); hitwhjpl@163.com (P.J.)
2 Shandong Institute of Shipbuilding Technology, Weihai 264209, Shandong, China
3 School of Mechatronics Engineering, Harbin Institute of Technology, Harbin 150001, Heilongjiang, China; hitzhangzhigang@163.com (Z.Z.); 18463103105@163.com (Z.W.)
* Correspondence: ww9965@hit.edu.cn; Tel.: +86-0631-5687830

Received: 17 January 2020; Accepted: 1 March 2020; Published: 5 March 2020

Abstract: The near-trapping phenomenon, which can lead to high wave elevations and large wave drift forces, is investigated by a floating four-column structure. To solve this wave-structure interaction problem, a numerical model is established by combining the wave interaction theory with a higher-order boundary element method. Based on this numerical model, behaviors of scattered waves at near-trapping conditions are studied; and the superposition principle of free-surface waves is introduced to understand this near-trapping phenomenon. To avoid the near-trapping phenomenon and protect the structure, a way for rotating the structure to change the wave-approach angle is adopted, and improvements of the wave elevations around the structure and the wave drift forces acting on each column are found. Moreover, a genetic-algorithm-based optimization method is adopted in order to minimize the total wave drift force acting on the whole structure at various wavenumbers by controlling the draft of floating bodies, the wave-approach angle and the separation distance between adjacent floating bodies. With the final optimized parameters, the wave drift forces both on each column and on the whole structure can be significantly reduced. The optimized arrangement obtained from a certain wavenumber can work not only at this target wavenumber but also at a range of wavenumbers.

Keywords: near-trapping; multiple floating bodies; wave drift force; wave-approach angle; optimization method

1. Introduction

The floating column-based structures always face complicated wave-structure interaction problems in ocean engineering [1]. In these problems, trapping phenomenon on structures occurring at certain wave frequencies means no waves scatter to infinity, which excites an oscillation of the water free surface in the vicinity of the structures and extreme wave forces on the structures. The trapped mode was first identified in an open channel by Ursell [2], and was proven by Callan [3] in the case of a submerged horizontal cylinder. Subsequently, trapping modes were observed by Maniar and Newman [4] in a large number of equally-spaced vertical cylinders located in a line. Motivated by Maniar and Newman [4], Evans and Porter [5] considered a number of bottom-mounted cylinders in circular configurations and firstly found the near-trapping phenomenon. They defined it as a local oscillation in the vicinity of the array at a well-defined frequency. At the near-trapping frequency, Evans and Porter [5] also found high wave elevations near the cylinders and large wave drift forces acting on each cylinder. Then, Jiang et al. [6] investigated the near-trapping phenomenon of four surface-piercing truncated cylinders to explain the relationship between the large wave drift forces on each cylinder and the high local wave elevations. Wang et al. [7] used a viscous-flow-based analysis method to study the viscous effects in the near-trapping phenomenon on a truncated four-cylinder structure. Investigations of the near-trapping have also been extended to second-order or much higher-order nonlinear wave diffraction problems. Malenica et al. [8] and Grice et al. [9] have semi-analytically studied the second-order diffraction of monochromatic waves by an array of bottom-seated cylinders and confirmed that the second-order waves can also be near-trapped in this type of cylinder array. Wang and Wu [10] employed a time domain method to analyze the near-trapping in an array of vertical cylinders. Bai et al. [11] used the fully nonlinear boundary element method to analyze the near-trapping phenomenon and proved the third-order excitation of near-trapping in these vertical cylinders. Cong et al. [12] showed the first-order and second-order wave elevations around the four vertical cylinders at the near-trapping frequency under different wave directions.

Recently, studies for avoiding the near-trapping phenomenon have attracted many researchers' interests. To avoid the near-trapping phenomenon at a certain frequency, Duclos and Clement [13] studied a disorder parameter to randomly displace the array of unevenly-spaced vertical cylinders from a regular array. Chen et al. [14] investigated the effects on the near-trapping due to the porosity of vertical cylinders and disorder of layout using the null-field integral equations. Evans and Porter [15] and Cong et al. [12] studied the effects of wave direction on the wave elevation and the exciting forces in the near-trapping modes of four bottom-mounted-columns; unfortunately, the effects on wave drift forces were not studied. To reduce the wave drift force and improve the hydrodynamic performance of the structures in waves, an optimization scheme is a powerful tool for this type of problem. Newman [16] used WAMIT and the multivariate optimizer PRAXIS to optimize the wave drift force on multiple truncated cylinders. He found that the scattered wave energy of the structure with a configuration that a truncated cylinder surrounded by several outer cylinders can be minimized almost to zero, which is known as the cloaking phenomenon. Following Newman's works, Iida et al. [17] minimized the wave drift force on the inner cylinder by adopting a binary-coded genetic algorithm developed by Tasrief and Kashiwagi [18]. By developing a real-coded genetic algorithm (GA), Zhang et al. [19] optimized the wave drift force on a structure that a truncated cylinder surrounded by four outer cylinders at various wavenumbers to achieve the cloaking phenomenon. Although the optimization method has been widely used for cloaking problems, it has been rarely introduced into the near-trapping problem.

Above all, some issues about the near-trapping phenomenon still require further studies. In this paper, the occurrence mechanism, wave direction effects on the wave drift force and the optimization method for near-trapping phenomenon are studied using four surface-piercing truncated cylinders. First, to investigate the mechanism of local oscillation of the water free surface at near-trapping frequencies, the behaviors of scattered waves and the superposition principle of waves are studied based on a combination of the wave interaction theory and the higher-order boundary element method. Second, a way for rotating the structure to change the wave-approach angle is conducted to avoid the near-trapping modes. A significant reduction of wave drift forces on each cylinder is found. Third, to reduce the wave drift force on the whole structure, the real-coded genetic algorithm developed by Zhang et al. [19] is adopted at near-trapping frequency by controlling the dimension of the structure and the angle of wave approach. It is found that the wave drift force not only on the whole structure but also on each column can be reduced for the optimized arrangement. Finally, the optimizations of the structural dimension and wave-approach angle are conducted at various wavenumbers to reduce the wave drift force on the whole structure. It is found that the optimized arrangement obtained from a certain wavenumber can work not only at this target wavenumber but also at a range of wavenumbers.

2. Theory

In this study, the wave interaction theory [20] is adopted to model this wave-structure interaction problem, while a higher-order boundary element method [21] is introduced as a numerical tool to discrete the equations. For the optimization problem, a real-coded genetic algorithm [19] is used to build the optimization scheme.

2.1. Structural Arrangement

A configuration of four identical truncated cylinders is considered, as shown in Figure 1. Each cylinder locates regularly with a distance, L, from the coordinate origin. The incident wave comes from the direction of the negative x-axis. The wave-approach angle β, of the four-column structure changes clockwise.

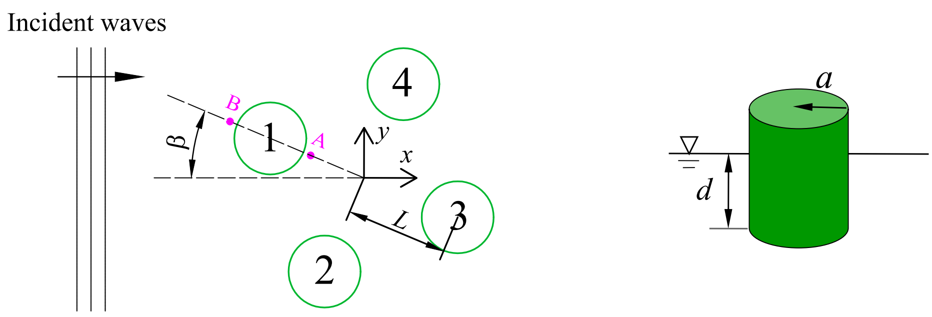

(**a**) Top view (**b**) Perspective view

Figure 1. Notation of parameters: (**a**) wave-approach angle β and parameter L; (**b**) radius a and draft d of the cylinders.

The radius a of the cylinders is fixed ($a = 1.0$ m). The draft d of the cylinders and the parameter L and the wave-approach angle β, as shown in Figure 1, are set as variables to optimize the wave drift force on the whole structure in the following optimization process. All geometric dimensions of the cylinders are normalized with respect to the radius a of the cylinders.

2.2. Wave Drift Force and Wave Elevation

This wave-structure interaction problem is solved based on the linear potential theory, while the Laplace's equation is taken as the governing equation of the flow field.

$$\nabla^2\Phi\,(x, y, z; t) = 0 \tag{1}$$

The linearized boundary conditions that are satisfied by the velocity potential are summarized as follows:

$$[F]\,\frac{\partial^2\Phi}{\partial t^2} + g\frac{\partial\Phi}{\partial z} = 0\,,\ \text{at}\ z = 0 \tag{2}$$

$$[H]\,\frac{\partial\Phi}{\partial n} = 0\,,\ \text{on the surface of a cylinder} \tag{3}$$

$$[B]\,\frac{\partial\Phi}{\partial z} = 0\,,\ \text{at}\ z = h \tag{4}$$

where, F, H and B denote the free surface condition, the body surface condition and the water bottom condition, respectively; h denotes the water depth and deep water condition considered in this paper.

Using the wave interaction theory, besides the global coordinate system $o - xyz$, the local coordinate systems $o_n - x_n y_n z_n$ fixed at the center of the n-th cylinder is used, as shown in Figure 2. A Cartesian coordinate systems of the form $o_n - x_n y_n z_n$ and a cylindrical coordinate system $o - r\theta z$

are both adopted. The positive direction of the z-axis is in the downward vertical direction, and the origin of each coordinate system ($z = 0$) is spaced on an undisturbed free surface.

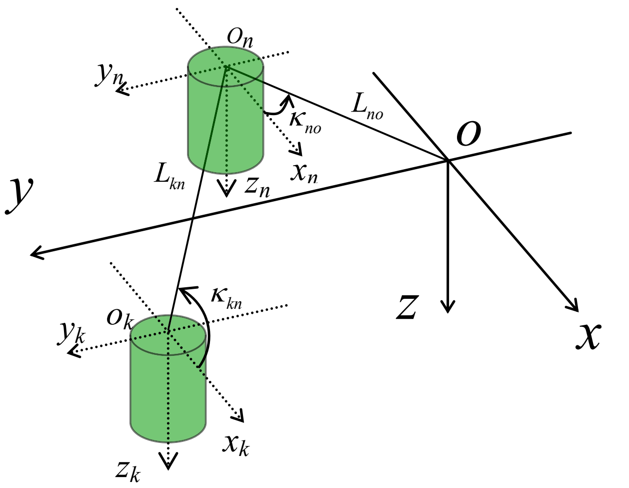

Figure 2. Global and local coordinate systems.

Based on the principle of linear superposition, the velocity potential can be expressed as follows:

$$\Phi(x, y, z; t) = \mathrm{Re}[\frac{g\zeta_0}{i\omega}\varphi(P)e^{i\omega t}] \tag{5}$$

where

$$\varphi(P) = \varphi_I(P) + \psi(P) \tag{6}$$

Here, Re[ ] in Equation (1) means the real part to be taken; ω and ζ_0 denote the circular frequency and amplitude of the incident waves, respectively; g is the gravitational acceleration; $P = (r, \theta, z)$ is a field point in the flow; In Equation (2), $\varphi(P)$ is the sum of the incident-wave potential $\varphi_I(P)$ and disturbance potential $\psi(P)$. The cylinders are assumed to be fixed, and only the diffraction problem is considered.

The linear regular waves are considered, and the incident-wave is assumed to come from the negative x-axis; therefore, the incident potential $\varphi_I(P)$ can be introduced in a cylindrical coordinate as follows:

$$\begin{aligned} \varphi_I(P) &= \frac{\cosh k_0(z-h)}{\cosh k_0 h} e^{-ik_0 x} \\ &= \sum_{m=-\infty}^{\infty} \alpha_m Z_0(z) J_m(k_0 r) e^{-im\theta} \end{aligned} \tag{7}$$

where

$$\alpha_m = e^{-im\pi/2},\ Z_0(z) = \frac{\cosh k_0(z-h)}{\cosh k_0 h} \tag{8}$$

$$K = \frac{\omega^2}{g} = k_0 \tanh k_0 h \tag{9}$$

Here, the Bessel function of the first kind of order m is denoted by $J_m(k_0 r)$.

The disturbance potential, due to the presence of multiple floating bodies in the incident waves, is denoted as $\psi(P)$. As derived in Kagemoto and Yue [20], the total disturbance potential $\psi(P)$ for a four-column structure can be expressed as:

$$\psi(P) = \sum_{n=1}^{4} \psi^n(P) \approx \sum_{n=1}^{4} \sum_{l=-\infty}^{\infty} A_l^n Z_0(z) H_l^{(2)}(k_0 r_n) e^{-il\theta_n} \tag{10}$$

Under an assumption of wide-spacing approximation [20], only progressive waves are considered in Equation (10), while the evanescent waves are neglected. Here, A_l^n denotes the complex amplitude of the scattered progressive waves around the n-th cylinder. A_l^n can be solved by a higher-order boundary element method reported in Kashiwagi [21]. The second kind of Hankel function of order l is denoted by $H_l^{(2)}(k_0 r_n)$.

Rewriting the disturbance potential in the global cylindrical coordinate systems, using the Graf's addition theorem for Bessel function, $\psi(P)$ can be given in the following form:

$$\psi(P) = \sum_{m=-\infty}^{\infty} A_m Z_0(z) H_m^{(2)}(k_0 r) e^{-im\theta} \tag{11}$$

where

$$A_m = \sum_{n=1}^{4} \sum_{l=-\infty}^{\infty} A_l^n J_{l-m}(k_0 L_{no}) e^{-i(l-m)\kappa_{no}} \tag{12}$$

Then, the entire velocity potential can be introduced as the sum of the incident-wave potential and the disturbance-wave potential.

$$\varphi(P) = \varphi_I(P) + \psi(P) = \sum_{m=-\infty}^{\infty} [\alpha_m J_m(k_0 r) + A_m H_m^{(2)}(k_0 r)] Z_0(z) e^{-im\theta} \tag{13}$$

Based on the velocity potential expressed in cylindrical coordinate systems, the total wave drift force acting on the entire cylinders can be obtained using the far-field method initiated by Maruo [22].

$$\frac{F_x^{total} - iF_y^{total}}{\rho g \zeta_0^2 a/2} = \frac{i}{C_0 K r} \sum_{m=-\infty}^{\infty} [2A_m A_{m+1}^* + \alpha_m A_{m+1}^* + \alpha_{m+1}^* A_m] \tag{14}$$

Performing the same analytical method in the n-th local coordinate system, the velocity potential around the n-th cylinder can be written as follows:

$$\begin{aligned} \varphi^n(P) &= \psi_I^n(P) + \psi^n(P) = (\varphi_I^n(P) + \sum_{k=1,k\neq n}^{4} \psi^{kn}(P)) + \psi^n(P) \\ &= \sum_{m=-\infty}^{\infty} [(\alpha_m^n + \sum_{k=1,k\neq n}^{4} A_m^{kn}) J_m(k_0 r_n) + A_m^n H_m^{(2)}(k_0 r_n)] \\ &\times Z_0(z) e^{-im\theta_n} \end{aligned} \tag{15}$$

where

$$A_m^{kn} = \sum_{l=-\infty}^{\infty} A_l^k H_{l-m}^{(2)}(k_0 L_{kn} e^{-i(l-m)\kappa_{kn}}) \tag{16}$$

$$\alpha_m^n = \alpha_m e^{-ik_0 x_{on}} \tag{17}$$

Then, the wave drift force acting on the n-th $(n = 1,2,3,4)$ individual cylinder can be written as:

$$\begin{aligned}\frac{F_x^n - iF_y^n}{\rho g \zeta_0^2 a/2} =& \frac{i}{C_0 Kr} \sum_{m=-\infty}^{\infty} \{2A_m^n A_{m+1}^{n*} + (\alpha_{m+1}^{n*} + \sum_{k=1,k\neq n}^{4} A_{m+1}^{kn*})A_m^n \\ &+ (\alpha_m^n + \sum_{k=1,k\neq n}^{4} A_m^{kn})A_{m+1}^{n*}\}\end{aligned} \tag{18}$$

where

$$C_0 = \frac{k_0}{K + (k_0^2 - K^2)h} \tag{19}$$

Here, the asterisk $*$ in the superscript denotes the complex conjugate.

The wave elevation can be obtained from the velocity potential. The velocity potential can be expressed as follows.

$$\Phi = \mathrm{Re}[\frac{g\eta_0}{2i\omega}\varphi e^{i\omega t}] \tag{20}$$

Based on the dynamic boundary condition, the wave elevation η^p can be obtained as

$$\eta^p = \mathrm{Re}[\eta_0 \varphi e^{i\omega t}] \tag{21}$$

The velocity potential can be written in the form of $\varphi = \varphi_c + i\varphi_s$, and the wave elevation can be expressed as

$$\begin{aligned}\frac{\eta^p}{\eta_0} &= \mathrm{Re}[(\varphi_c + i\varphi_s)e^{i\omega t}] = \sqrt{\varphi_c^2 + \varphi_s^2}\cos(\omega t + \arctan\frac{\varphi_s}{\varphi_c}) \\ &= \frac{\eta}{\eta_0}\cos(\omega t + \arctan\frac{\varphi_s}{\varphi_c})\end{aligned} \tag{22}$$

Here, $\frac{\eta}{\eta_0}$ denotes the non-dimensional wave elevation.

2.3. Description of GA

A real-coded Genetic Algorithm (RGA) proposed in Zhang et al. [19] is adopted to minimize the wave drift force acting on the four-column structure by optimizing the dimensions of the structure. The set-up of this algorithm is as follows:

2.3.1. Initial Population

A series of initial individuals composed of variables are generated randomly in the search space. An individual denotes a potential solution to the problems. In this study, the number of the initial individuals is 100.

2.3.2. Operators

Genetic algorithm (GA) is an intelligent optimization algorithm, which mimics the process of natural selection. The roulette selection operator, the real-value crossover, the real-value mutation operator and elitism are employed in this study. Here, elitism means that the best individual composed of certain variables can always be reserved to avoid being broken by the crossover and the mutation operators.

2.3.3. Variables and Objective Function

In the present optimized progress, three dimensional parameters d, L and β are selected as the variables, while the absolute value of the wave drift forces acting on the whole structure is selected as the objective function. By optimizing d, L and β, the minimized wave drift force on the four-column structure can be obtained.

2.3.4. Constraints

The arrangements of the four cylinders are limited to the geometric constraints that the adjacent cylinders can not overlap. The locations of the four cylinders are decided by L and a. Thus, the constraints of these two variables can be mathematically described as follows, $\sqrt{2}L > 2a$.

2.3.5. Termination Conditions

The optimization process can be terminated if any following conditions are satisfied: (1) the elite values of the objective are not improved in more than 30 generations. (2) The number of generations is larger than 100.

3. Numerical Results and Discussion

As mentioned, a higher-order boundary element method is adopted to obtain the complex amplitude A_l^n for the n-th (n = 1, 2, 3, 4) cylinder. The Green function satisfying the free-surface condition is used, only the surface of the truncated cylinders should be discretized.

3.1. The Near-Trapping on the Four-Column Structure

A four-column structure with the dimensions shown in Table 1, which is the same as that in Jiang et al. [6], was considered. The resultant wave drift forces $F^n = \sqrt{(F_x^n)^2 + (F_y^n)^2}$ acting on the n-th $(n = 1, 2, 3, 4)$ cylinder against a range of wavenumbers were calculated, as shown in Figure 3. It can be noted that the wave drift forces acting on each cylinder, seeing Figure 3, simultaneously become large at the same wavenumber $k_0 a \approx 1.68$, which is known as the near-trapping frequency.

Table 1. The configuration of the four-column structure.

L	β	d	a
$2\sqrt{2}$	0°	3.0	1.0

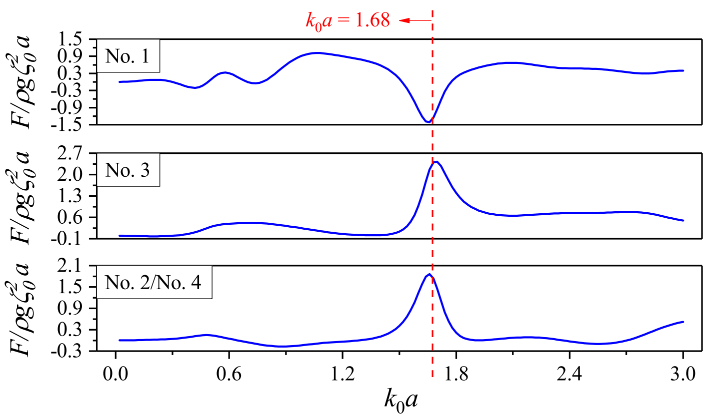

Figure 3. The wave drift forces acting on each cylinder.

As is known, associating with this extreme phenomenon, the local resonance of the water free surface can be excited. The dimensionless wave elevation at $k_0 a = 1.68$ was calculated and shown in Figure 4a. The wave profile of the No. 3 cylinder at the near-trapping mode in the local coordinate system $o_3 - x_3 y_3 z_3$ is presented in Figure 4b, and the corresponding wave profile of a single cylinder is also plotted for comparison.

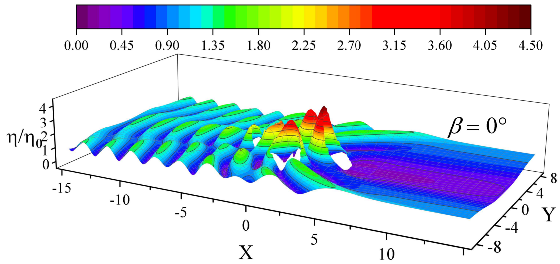

(a)

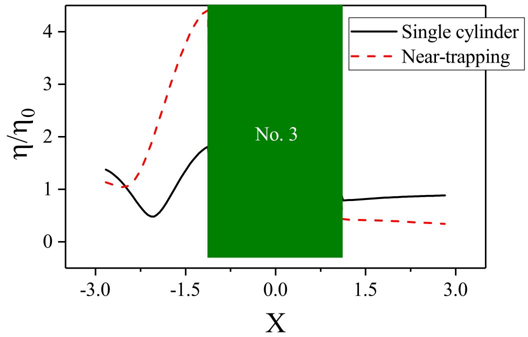

(b)

Figure 4. The dimensionless free-surface elevation at $k_0a = 1.68$: (**a**) perspective view; (**b**) profile of the No. 3 cylinder.

From Figure 4a, it can be found that the run-up on the cylinders inside the structure is very large. The maximum wave elevation in the weatherside of the No. 3 cylinder is more than 4.4 times of the incident waves, which can be obviously seen from Figure 4b; however, the wave elevation is close to zero in the leeside of the structure, which means nearly no waves scatter to far field. Here, the local wave resonance of run-up on the cylinder may be easily over-estimated due to ignoring the nonlinear and viscous effects. To obtain an exact result for the extreme run-up, a nonlinear theory considering the viscosity of the fluid should be carefully introduced.

To further understand the "trapping" of waves, the dimensionless scattered-wave elevation at $k_0a = 1.68$ is calculated and shown in Figure 5a, while the scattered-wave profile of the No. 3 cylinder in the local coordinate system $o_3 - x_3y_3z_3$ is shown in Figure 5b. A local resonance of the scattered waves can also be found in Figure 5a,b, while the scattered-wave elevation in the leeside of the structure is not zero, which means some scattered waves radiate to the far field. It is interesting that the total wave in Figure 4b almost does not scatter to the far field, while the scattered wave in Figure 5b radiates.Therefore, this difference between the free-surface elevation and the scattered-wave elevation in the leeside of the structure needs to be studied.

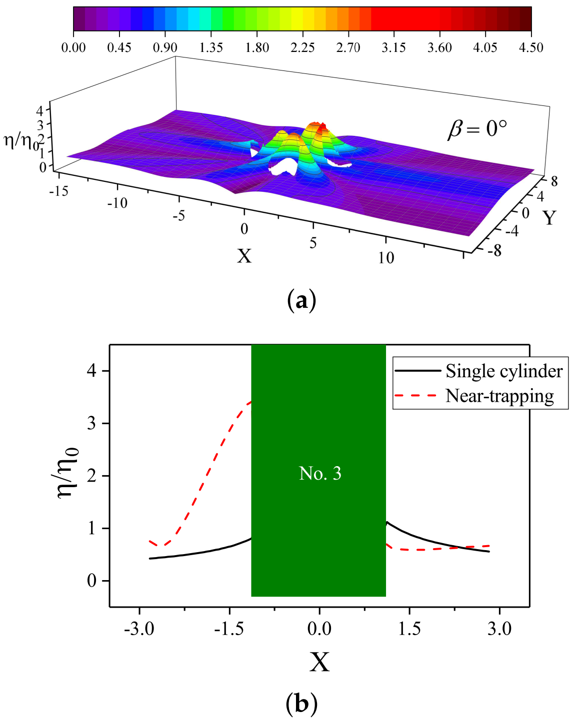

Figure 5. The dimensionless scattered-wave elevation at $k_0a = 1.68$: (**a**) perspective view; (**b**) profile of the No. 3 cylinder.

The superposition principle of the water free surface is adopted to explain the above-mentioned contradiction. As known, the water free surface can be regarded as the superposition of the incident waves and the scattered waves. The distribution of free surface elevation $\frac{\eta^p}{\eta_0}$ at $k_0a = 1.68$ with consideration of the initial phase was calculated by Equation (22), as shown in Figure 6.

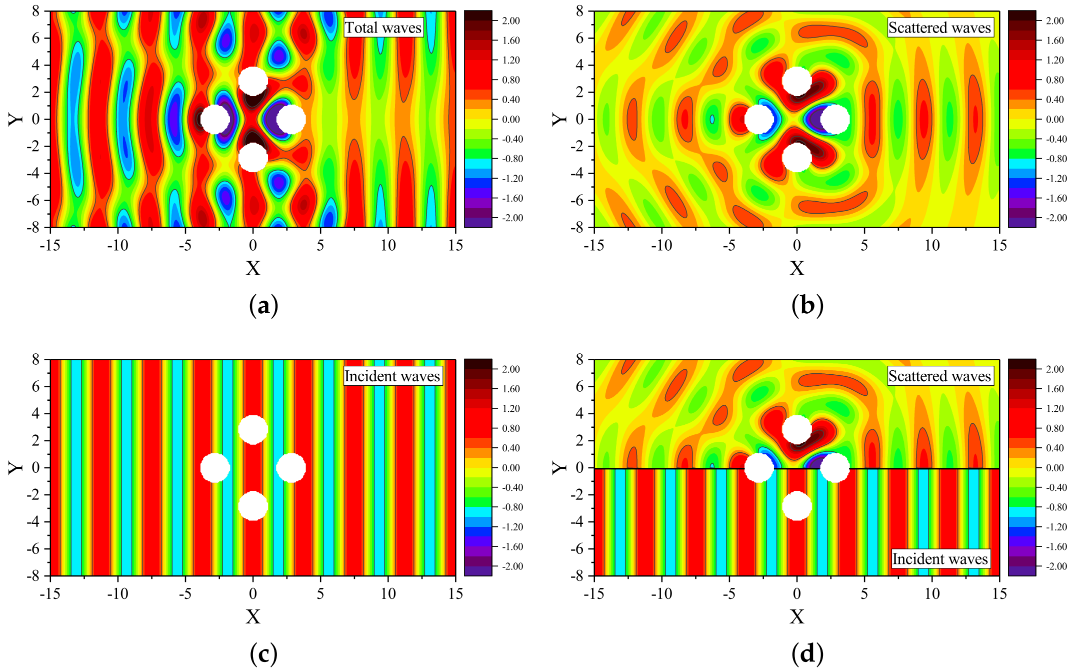

Figure 6. The wave elevation η^p/η_0 considering the initial phase at $k_0a = 1.68$: (**a**) total waves; (**b**) scattered waves; (**c**) incident waves; (**d**) scattered waves and incident waves.

Figure 6a shows the results of the total free surface. The peaks of free surface near No. 2 and No. 4 cylinders can be found with the troughs of free surface near No. 1 and No. 3 cylinders, which demonstrates that the peaks and the troughs of this local resonance coexist at the near-trapping frequency. Moreover, almost zero wave elevation in the leeside of the structure can be observed in Figure 6a.

Figure 6b shows the results of the scattered waves. The peaks and the troughs inside the structure have the same trends as that of the total free surface shown in Figure 6b, but the scattered-wave elevation in the leeside is obviously not zero. This phenomenon was also mentioned and clearly seen in Figures 4b and 5b.

Figure 6c shows the results of the incident waves. To analyze the superposition between the scattered waves and the incident waves, the half contents respective in Figure 6b,c are drawn in one figure, as shown in Figure 6d. In Figure 6d, the upper part is the results of the scattered waves, while the lower part is the results of the incident waves. From Figure 6d, the phase difference between the scatted waves and the incident waves is obviously found, and it shows great effects on the near-trapping phenomenon. The mutual promotion between the scattered waves and the incident waves inside the structure can be observed, while the cancellation effects between the scattered waves and the incident waves can be visibly found, which explained the small wave elevation in the leeside of the structure as shown in Figure 4a.

3.2. Avoid Near-Trapping by Changing Wave-Approach Angle

Based on the idea of breaking the symmetry of the structure about the wave direction to destroy the near-trapping mode ($k_0a = 1.68$), a means of rotating the structure to change the wave-approach angle, β, was adopted. In this simulation, the other two parameters (L, d) of the four-column structure, shown in Table 1, are fixed. The wave elevations and the wave drift forces of the four-column structure at three conditions $\beta = 15°, \beta = 30°, \beta = 45°$ were analyzed in these studies. For the convenience of the following comparisons, the free-surface elevation and the scattered-wave elevation of a single cylinder ($a = 1.0$, $d = 3.0$) at $k_0a = 1.68$ are, respectively, shown in Figures 7 and 8.

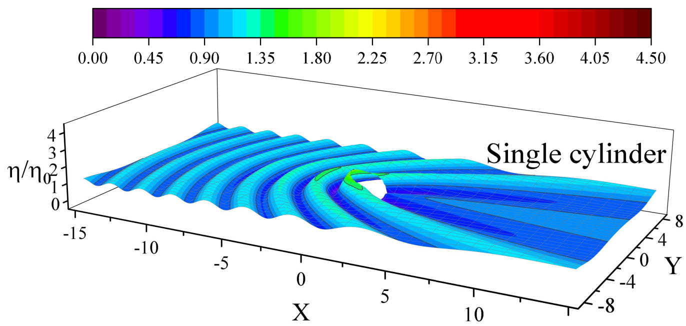

Figure 7. The free-surface elevation η/η_0 of single cylinder at $k_0a = 1.68$.

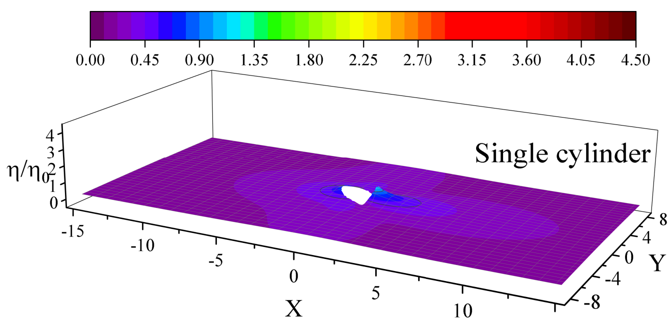

Figure 8. The scattered-wave elevation of single cylinder at $k_0a = 1.68$.

The free-surface elevation and the scattered-wave elevation of the four-column structure at $k_0a = 1.68$ against three wave-approach angles were calculated and shown in Figure 9. In Figure 9, the upper three subgraphs are, respectively, the dimensionless free-surface elevations of $\beta = 15°$, $\beta = 30°$, $\beta = 45°$, while the lower three subgraphs are the scattered-wave elevations. From Figure 9, it can be seen that the local resonances inside the structure disappear while those are clearly seen in Figures 4 and 5. Especially for $\beta = 15°$, the behavior of the free surface and the scattered waves are more like that of the single cylinder shown in Figures 7 and 8.

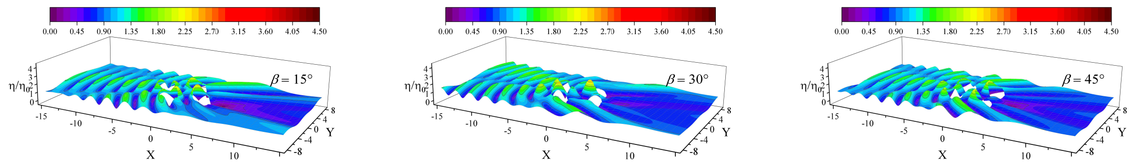

(**a**) free-surface elevations

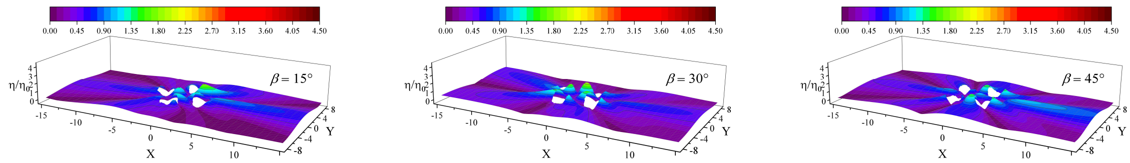

(**b**) scattered-wave elevations

Figure 9. The free-surface and scattered-wave elevations of the four-column structure at $k_0a = 1.68$ against three different wave-approach angles.

Next, the resultant wave drift forces on each cylinder at different wave-approach angles were calculated and analyzed. Figure 10a shows the results of the original structure ($\beta = 0°$), in which very large wave drift forces are found due to the near-trapping that occurred at $k_0a = 1.68$. From Figure 10b–d, it can be found that the extreme wave drift forces on each cylinder disappear at $k_0a = 1.68$ for $\beta = 15°, \beta = 30°, \beta = 45°$. Moreover, the maximal wave drift forces do not even occur on each column at the range of $0 < k_0a < 3.0$, not just at $k_0a = 1.68$, as shown in Figure 10b–d, which means the way of changing the wave-approach angle can play a significant role in destroying near-trapping modes.

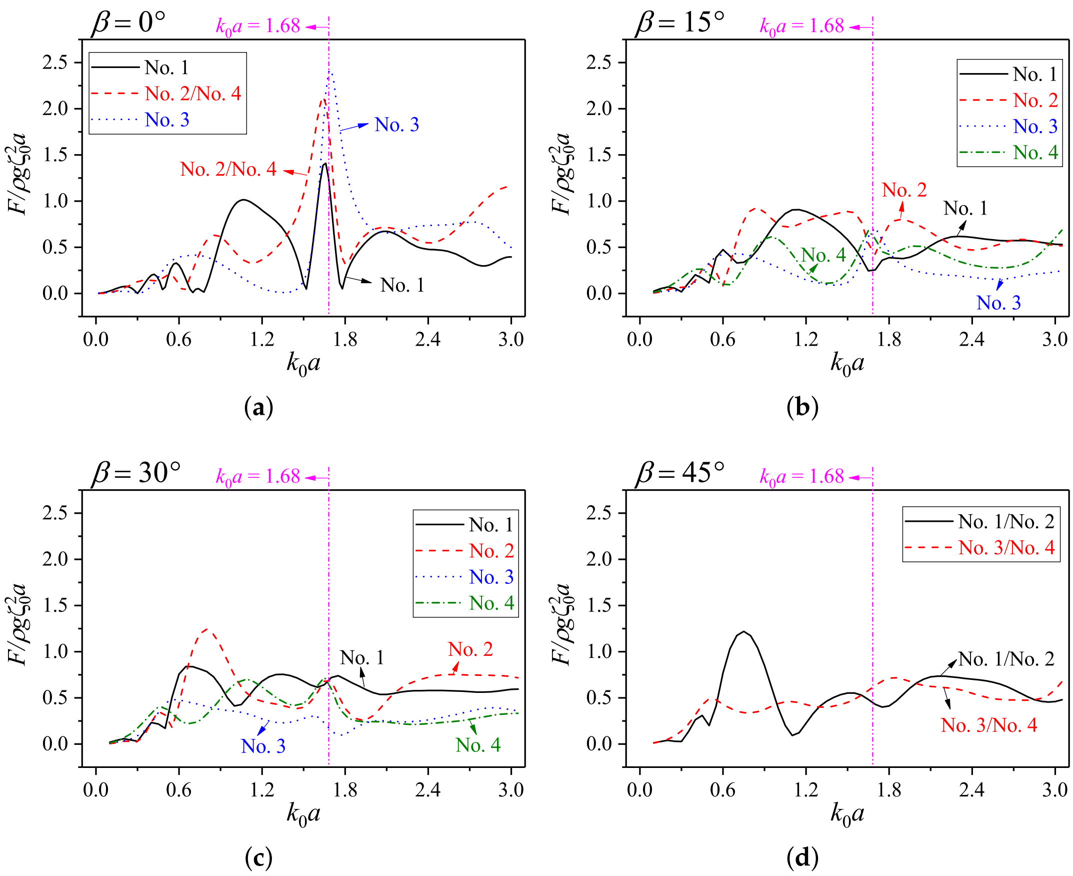

Figure 10. The wave drift forces on each cylinder against four different wave-approach angles: (**a**) $\beta = 0°$, (**b**) $\beta = 15°$, (**c**) $\beta = 30°$, (**d**) $\beta = 45°$.

Focusing on the wave drift forces at $k_0a = 1.68$ shown in Figure 10, Figure 11 is drawn. Figure 11 presents the values of wave drift forces acting on each column against different wave-approach angles at $k_0a = 1.68$, while the percentage in the bracket means the ratios between the decrement of wave drift force on each cylinder due to the change of wave-approach angle and the wave drift forces on the corresponding cylinder at $\beta = 0°$. The maximum wave drift forces can be found at $\beta = 0°$ for each cylinder. Due to the change of wave-approach angle, the wave drift forces on each cylinder are significantly reduced. For example, the wave drift force acting on the No.1 cylinder at $\beta = 0°$ ($F^1 = 1.2562$) is reduced by 83% to 0.2174 if the wave-approach angle changes to $\beta = 15°$.

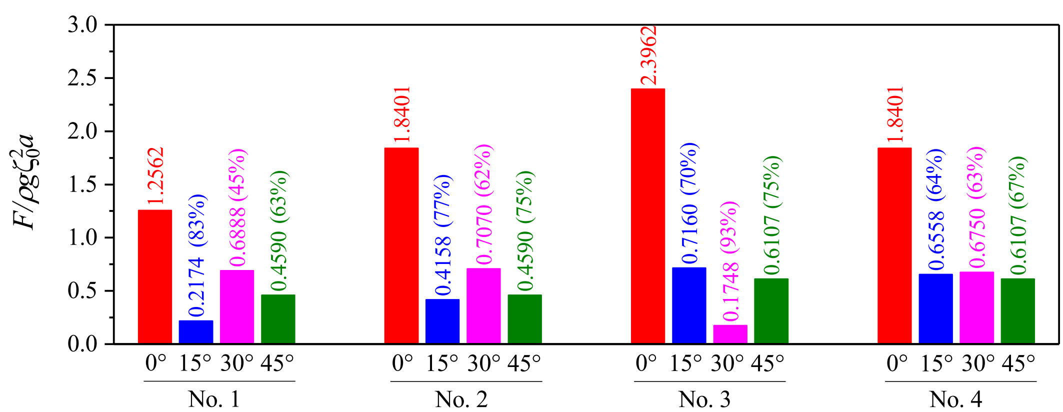

Figure 11. The wave drift forces on each cylinder against four different wave-approach angles and the corresponding decrement percentage at $k_0a = 1.68$.

Then, the total wave drift forces $F^{total} = \sqrt{(F_x^{total})^2 + (F_y^{total})^2}$ acting on the whole structure over a wide range of wavenumbers were calculated, as shown in Figure 12. It can be found that the wave drift forces on the whole structure can not be significantly reduced at $k_0 a = 1.68$ like that of the wave drift force on each cylinder just by changing the wave-approach angle. Moreover, the wave drift forces become larger for long waves $(0.5 < k_0 a < 0.9)$ when the wave-approach angle changes from $\beta = 0°$, which implies that the way of just changing the wave-approach angle to reduce the wave drift forces on the whole structure needs to be carefully employed.

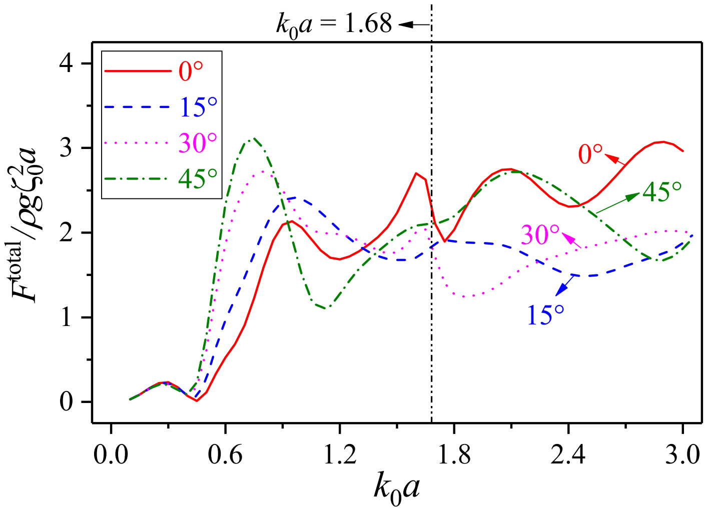

Figure 12. The total wave drift forces on the whole structure with different wave-approach angles.

Figure 13 shows the comparison of the wave drift forces on the whole structure between different wave-approach angles at $k_0 a = 1.68$. The minimum value can be found at $\beta = 15°$. It should be noted that the way of changing wave-approach angles to reduce the wave drift forces at $k_0 a = 1.68$ is limited; even for the best case, $\beta = 15°$, the reduction of the wave drift forces on the whole structure is limited at 20%. Thus, an optimization method seems needed to significantly reduce the wave drift forces on the whole structure, which will be treated in the following subsections.

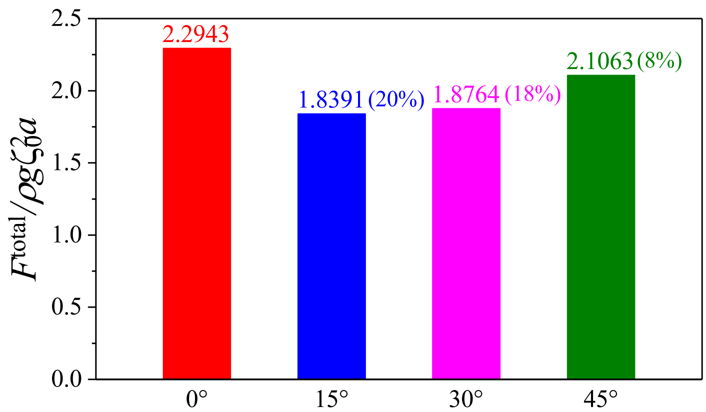

Figure 13. The total wave drift forces on the whole structure with different wave-approach angles and the corresponding decrement percentage at $k_0 a = 1.68$.

3.3. Optimization of Wave Drift Force on the Whole Structure

To reduce the wave drift force both on the whole structure and on each cylinder, a real-coded optimization algorithm developed by Zhang et al. [19] is adopted. The optimal variables chosen to minimize the wave drift force F^{total} are the wave-approach angle β, the length parameter L and the draft d of cylinders, which are defined in Figure 1. The optimization for $k_0 a = 1.68$ was firstly conducted, and the initial ranges of three variables are $0^\circ \leq \beta \leq 45^\circ, 2.0 \leq L \leq 4.5, 2.0 \leq d \leq 3.5$. The final optimized variables and the corresponding wave drift force on the whole structure are shown in Table 2. In this study, using Intel Core I7-4790 (3.60 GHz), the running time of an objective function evaluation is about 15 s, and the average time in obtaining the optimized results for one wavenumber is about 19 h.

Table 2. The optimized results of the variables and the corresponding wave drift force.

$k_0 a$	L	β	d	F^{total}
1.68	3.2694	25.9169°	2.0021	1.0945

Figure 14 shows comparisons of the total wave drift forces on the whole structure between the optimized configuration shown in Table 2 and the original one shown in Table 1. Figure 14 also presents four times of the wave drift force acting on the single cylinder ($a = 1.0$, $d = 3.0$). The reduction of wave drift forces at $k_0 a = 1.68$ by the optimized method can be apparently found.

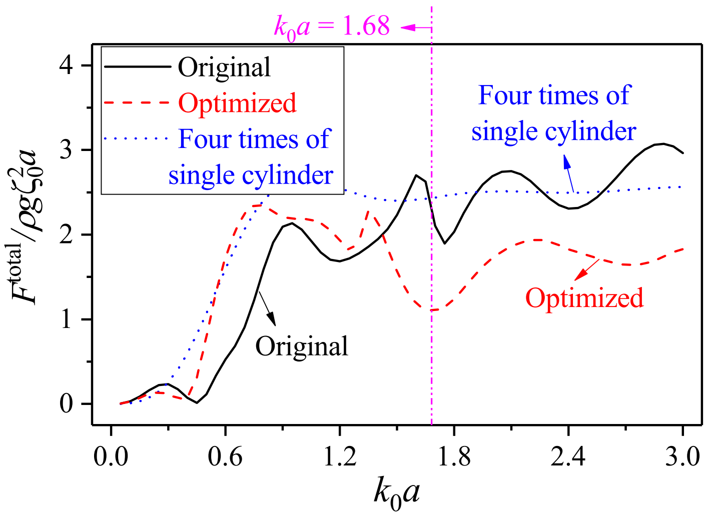

Figure 14. The total wave drift forces on the original structure, optimized structure and four times of single cylinder.

Figure 15 shows the corresponding comparison of the total wave drift forces at $k_0 a = 1.68$ between the original structure, optimized structure, four times of single cylinder. The optimized wave drift force can be significantly decreased by 52% of the original wave drift force and 55% of the four times of the single cylinder.

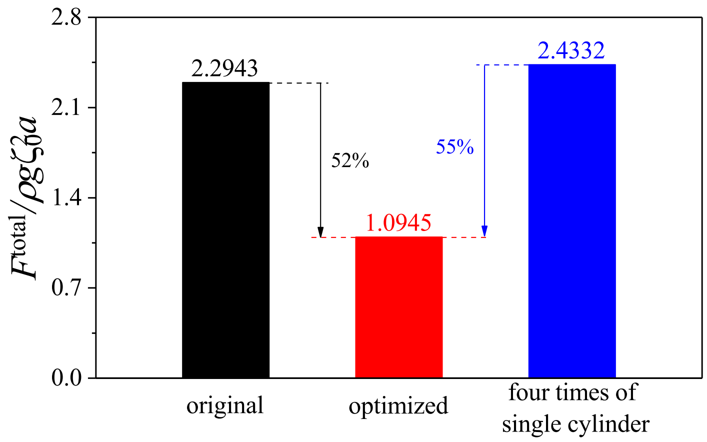

Figure 15. The total wave drift forces on the original structure, optimized structure and four times of single cylinder at $k_0a = 1.68$.

Then, the free-surface elevation and the scattered-wave elevation at $k_0a = 1.68$ were calculated for the optimized structure, as shown in Figures 16 and 17. From Figures 16 and 17, it can be found that the local resonance of the free-surface and the scattered waves disappears, and the wave patterns near each cylinder are like that of the single cylinder shown in Figures 7 and 8.

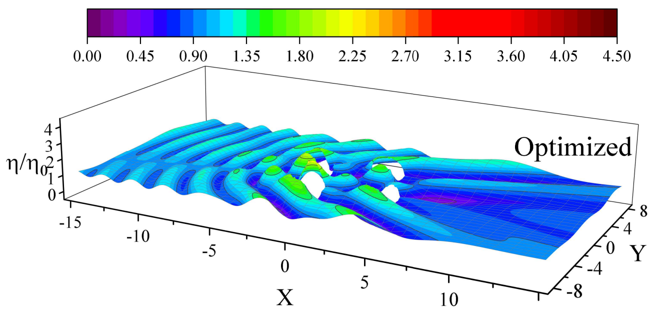

Figure 16. The free-surface elevation of optimized structure at $k_0a = 1.68$.

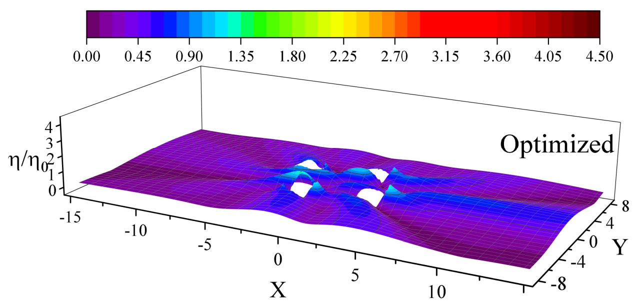

Figure 17. The scattered-wave elevation of optimized structure at $k_0a = 1.68$.

Next, the wave drift forces on each cylinder of the optimized structure were calculated and shown in Figure 18. Compared with Figure 10a, the resonance of wave drift forces at $k_0a = 1.68$ also disappears, which means this optimized configuration for minimizing the wave drift force on the whole structure can also reduce the wave drift forces acting on each cylinder. Moreover, the resonance of the wave drift forces can not be found in the range of $0 < k_0a < 3.0$.

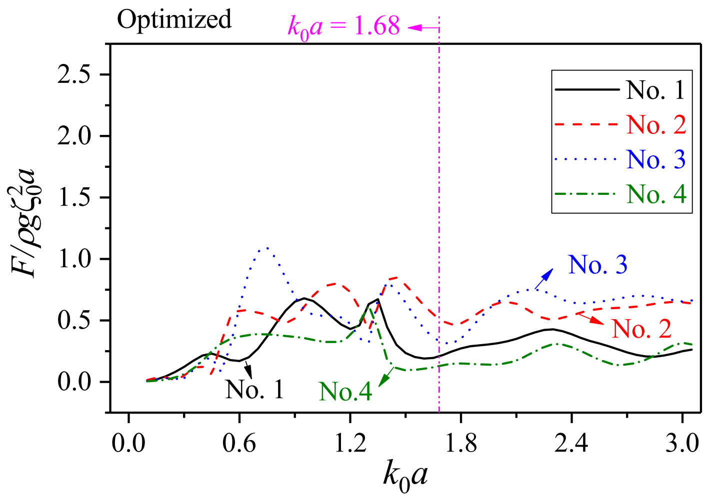

Figure 18. The wave drift forces on each cylinder with optimized structure.

To quantitatively show the reduction of the wave drift force on each cylinder, the values of the wave drift force on each cylinder for the original and optimized structures at $k_0a = 1.68$ were compared and shown in Figure 19. From Figure 19, it can be found that the wave drift forces on each cylinder are also being significantly reduced by this optimization.

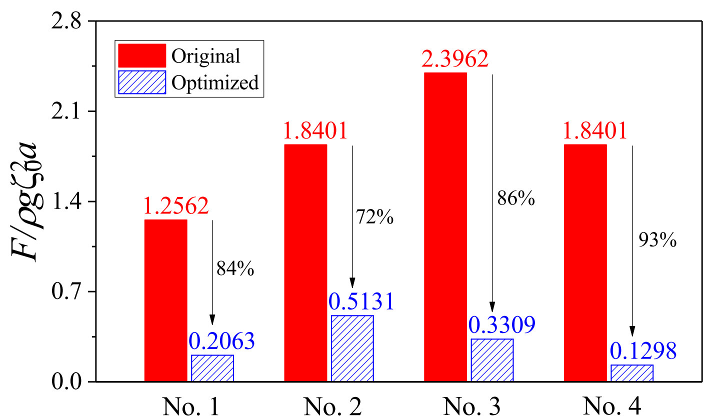

Figure 19. The wave drift forces on each cylinder for the original structure and the optimized structure at $k_0a = 1.68$.

To understand the reduction of wave drift force on each cylinder by the optimized method, wave profiles around each cylinder surface for the original structure and the optimized structure were calculated and analyzed at $k_0a = 1.68$ in local coordinate systems. The upper four subgraphs shown in Figure 20a are the wave profiles of each cylinder in the original structure at $k_0a = 1.68$, which corresponds to the near-trapping phenomenon, while the four subgraphs in Figure 20b show the wave profiles of each cylinder in the optimized structure. In each subgraph, the projections of the data onto the three coordinate planes are also presented. From these subgraphs, it can be found that the wave difference between two sides of each cylinder with optimized arrangement is very small, which contributes to the reduction of wave drift force shown in Figure 19. Therefore, the wave drift forces on each cylinder have a strong connection with the local waves near each cylinder.

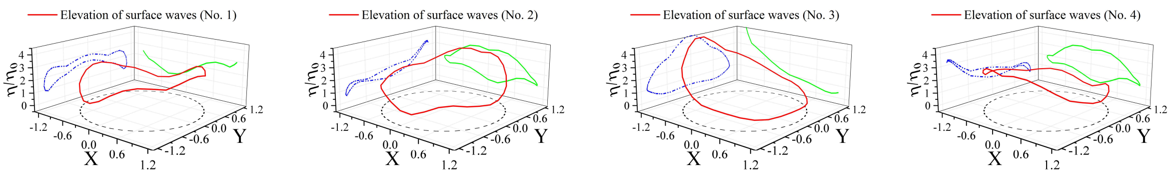

(**a**) the original structure

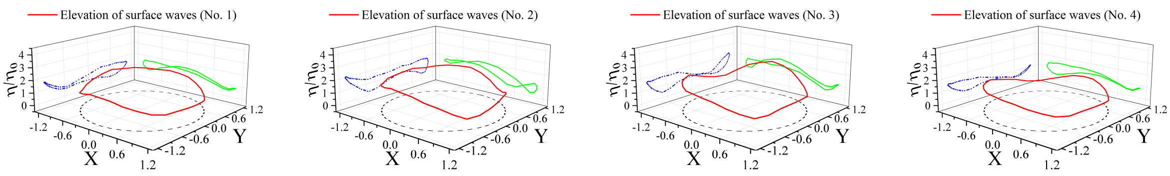

(**b**) the optimized structure

Figure 20. The free-surface and scattered-wave elevations of the four-column structure at $k_0a = 1.68$ against three different wave-approach angles.

Finally, the optimization method was applied to minimize the total wave drift force on the whole structure for four other different wavenumbers: $k_0a = 1.0, 1.2, 1.4, 1.8$. The final optimized values of three variables (β, L, d) obtained by the genetic algorithm (GA) and the corresponding wave drift forces F^{total} are shown in Table 3. In Table 3, the minimum gap ratio $(\sqrt{2}L/2a = 1.86)$ of adjacent cylinders can be obtained at the case of $k_0a = 1.2$, which still satisfies the wide-spacing approximation [20]. Therefore, the wave drift forces presented in Table 3 calculated based on this approximation are valid.

Table 3. The optimized results of the variables and the corresponding wave drift forces at $k_0a = 1.0, 1.2, 1.4, 1.8$.

k_0a	L	β	d	F^{total}		c
				Original	**Optimized**	
1.0	3.2188	44.8545°	2.5258	2.0594	0.9314	55%
1.2	2.6235	44.9831°	2.5089	1.6851	1.1728	30%
1.4	4.0762	26.3420°	2.7528	1.9467	1.1417	41%
1.8	3.0712	25.7292°	2.6103	2.0350	1.0945	46%

In Table 3, $c = (F^{total}(original) - F^{total}(optimized))/F^{total}(original)$ is used to define the reduction of the wave drift force by the optimized method. From Table 3, it can be found that the wave drift force F^{total} at each wavenumber is significantly reduced by the optimized method. For the case of $k_0a = 1.0$, the wave drift force on the whole structure can be decreased by 52%.

Figure 21 shows comparisons of the wave drift forces on the whole structure between the original structure and the optimized arrangements at four different wavenumbers. In Figure 21, the solid line denotes the wave drift forces on the original structure. It can be found that the wave drift force with optimized arrangements can be significantly reduced at each target wavenumber. It should be noted that the optimized arrangement obtained for a certain wavenumber can work not only at this target wavenumber but also at a range of wavenumbers close to this wavenumber. For example, the optimized arrangement obtained for $k_0a = 1.0$ can also work at $0.84 \leq k_0a \leq 1.18$, which means the optimization structure can be applied to wide frequencies close to the target frequency in the real sea.

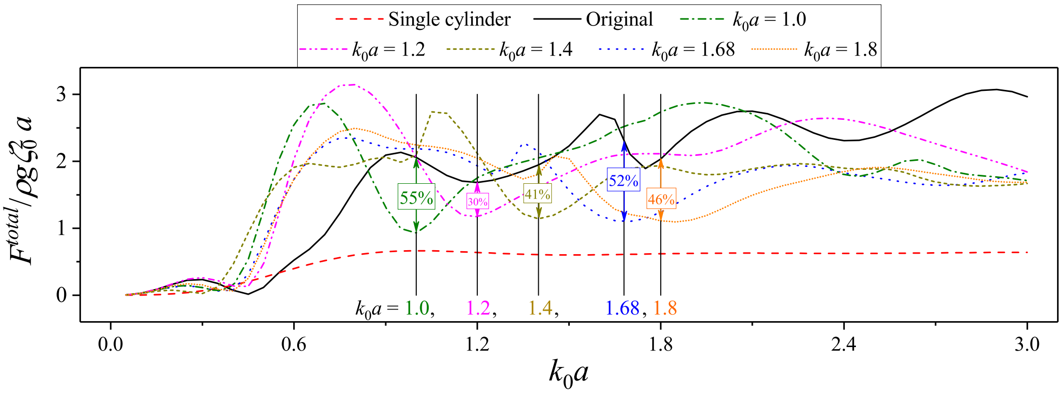

Figure 21. The total wave drift force for the original structure and the optimized structure.

4. Conclusions

With a combination of the higher-order boundary element method and the wave interaction theory, the near-trapping phenomenon on a four-column structure was studied by analyzing the behavior of scattered waves and the superposition principle of the free surface at the near-trapping mode. Then, to avoid this extreme phenomenon, the sensitivity of the wave-approach angle was investigated. Next, to reduce the wave drift forces on the whole structure, a real-coded genetic optimized algorithm was adopted to optimize three variables (β, L, d). The comparison of the performance of the wave drift force and the wave elevation between the original and optimized structures was conducted. Based on the present study, it can be concluded that:

1) The way of changing the wave-approach angle to avoid the near-trapping phenomenon is effective due to the fact that the symmetry of the structure is destroyed. The wave elevation, the wave drift forces on each cylinder can be improved at the near-trapping frequency by changing the wave-approach angle, while the decrease of the wave drift force on the whole structure is limited.
2) The reduction of the wave drift force not only on the whole structure at the $k_0a = 1.68$ but also on each cylinder by the optimized method was validated. The improvement of the wave elevation near the cylinder contributes to the reduction of the wave drift force acting on each cylinder.
3) The optimization method was applied to minimize the total wave drift force on the whole structure for four other different wavenumbers. It should be noted that the optimized arrangement obtained from a certain wavenumber can work not only at this target wavenumber but also at a range of wavenumbers, which means the optimization of structure can be applied to wide frequencies in practice.

Author Contributions: Conceptualization, G.H. and Z.Z.; methodology, Z.Z.; validation, W.W., Z.W. and P.J.; formal analysis, G.H.; investigation, Z.W.; writing—original draft preparation, Z.Z.; writing—review and editing, G.H.; visualization, Z.Z. and Z.W.; supervision, W.W.; project administration, G.H.; funding acquisition, G.H. All authors have read and agreed to the published version of the manuscript.

Funding: This work was supported by the National Natural Science Foundation of China (11502059); Natural Scientific Research Innovation Foundation in Harbin Institute of Technology (HIT. NSRIF. 201726); Shandong Province Key R&D Program (2019GHY112024).

Conflicts of Interest: The authors declare no conflict of interest.

Nomenclature

β	Wave approach angle
a	Radius of the cylinder
d	Draft of the cylinder
ω	Circular frequency of incident waves
h	Water depth
ρ	Water density
g	Gravitational acceleration
L	Distance between the cylinder and the coordinate origin
ζ_0	Amplitude of incident waves
η_0	Elevation of incident waves
η^p	Wave elevation considering phase
η	Wave elevation
F^n	Wave drift force on the n-th cylinder
k_0	Wave number
F^{total}	Wave drift force on the four cylinders
c	Reduction coefficient of F^{total} by optimized method

References

1. Faltinsen, O. *Sea Loads on Ships and Offshore Structures*; Cambridge University Press: Cambridge, UK, 1990.
2. Ursell, F. Trapping modes in the theory of surface waves. In *Mathematical Proceedings of the Cambridge Philosophical Society*; Cambridge University Press: Cambridge, UK, 1951; Volume 47, pp. 347–358.
3. Callan, M.; Linton, C.; Evans, D. Trapping modes in two-dimensional wave-guides. *J. Fluid Mech.* **1991**, *229*, 51–64. [CrossRef]
4. Maniar, H.; Newman, J. Wave Diffraction by a long array of cylinders. *J. Fluid Mech.* **1997**, *339*, 309–330. [CrossRef]
5. Evans, D.; Porter, R. Near-trapping of waves by circular arrays of vertical cylinders. *Appl. Ocean Res.* **1997**, *19*, 83–99. [CrossRef]
6. Jiang, S.; Lv, L.; Teng, B.; Gou, Y. Hydrodynamic analyses for near-trapping of a four-cylinder structures under water waves. *J. Harbin Eng. Univ. China* **2011**, *32*, 546–554.
7. Wang, Z.; He, G.; Zhang, Z.; Meng, Y. Viscous-flow-based analysis of wave near-trapped in a four-cylinder structure. *J. Mar. Sci. Appl.* **2018**, *17*, 371–379. [CrossRef]
8. Malenica, S.; Taylor, R.; Huang, J. Second-order water waves diffraction by an array of vertical cylinders. *J. Fluid Mech.* **1999**, *390*, 349–373. [CrossRef]
9. Grice, J.; Taylor, P.; Taylor, R. Near-trapping effects for multi-column structures in deterministic and random waves. *Ocean Eng.* **2013**, *58*, 60–77. [CrossRef]
10. Wang, C.; Wu, G. Time domain analysis of second-order wave diffraction by an array of vertical cylinders. *J. Fluids Struct.* **2007**, *23*, 605–631. [CrossRef]
11. Bai, W.; Feng, X.; Taylor, R.; Ang, K. Fully nonlinear analysis of near-trapping phenomenon around an array of cylinders. *Appl. Ocean Res.* **2014**, *44*, 71–81. [CrossRef]
12. Cong, P.; Gou, Y.; Teng, B.; Zhang, K.; Huang, Y. Model experiments on wave elevation around a four-cylinder structure. *Ocean Eng.* **2015**, *96*, 40–55. [CrossRef]
13. Duclos, G.; Clement, A. Wave propagation through arrays of unevenly spaced vertical piles. *Ocean Eng.* **2004**, *31*, 1655–1668. [CrossRef]
14. Chen, J.; Lin, Y.; Lee, Y.; Wu, C. Water wave interaction with surface-piercing porous cylinders using the null-field integral equations. *Ocean Eng.* **2011**, *38*, 409–418. [CrossRef]
15. Evans, D.; Porter, R. Near-trapping and trapping by arrays of cylinders in waves. *J. Eng. Math.* **1999**, *35*, 149–179. [CrossRef]
16. Newman, J. Cloaking a circular cylinder in water waves. *Eur. J. Mech. B/Fluid* **2014**, *47*, 145–150. [CrossRef]
17. Iida, T.; Kashiwagi, M.; He, G. Numerical confirmation of cloaking phenomenon array of floating bodies and reduction of wave drift force. *Int. J. Offshore Polar Eng.* **2014**, *24*, 241–246.

18. Tasrief, M.; Kashiwagi, M. Improvement of ship geometry by optimizing the sectional area curve with binary-coded genetic algorithms (BCGAS). In Proceedings of the 23th International Offshore and Polar Engineering Conference, Anchorage, AK, USA, 30 June–5 July 2013; pp. 869–875.
19. Zhang, Z.; He, G.; Wang, Z. Real-coded genetic algorithm optimization in reduction of wave drift forces on an array of truncated cylinders. *J. Mar. Sci. Technol.* **2019**, *24*, 930–947. [CrossRef]
20. Kagemoto, H.; Yue, D. Three-dimensional bodies in water waves: an exact algebraic method. *J. Fluid Mech.* **1986**, *166*, 189–209. [CrossRef]
21. Kashiwagi, M. An accurate calculation method for wave-induced steady force on multiple bodies. *Trans. West-Jpn. Soc. Nav. Archit. Bull Res. Inst. Appl. Mech. Kyushu Univ. Jpn.* **1995**, *78*, 83–98.
22. Maruo, H. The drift of a body floating on waves. *J. Ship Res.* **1960**, *4*, 1–10.